International Journal of Science and Research (IJSR)
ISSN: 2319-7064
Impact Factor 2025: 7.089

ANFIS Based Energy Management and Harmonic Reduction in an Islanded Hybrid Renewable Energy Microgrid System

Devireddy Sathish[1], Pannala Krishna Murthy[2], Narri Yadaiah[3]

[1]Department of Electrical and Electronics Engineering, Jawaharlal Nehru Technological University, Hyderabad, India
Corresponding Author Email: *data.sathish[at]gmail.com*

[2]Department of Electrical and Electronics Engineering, Jayaprakash Narayan College of Engineering, Mahabubnagar, India.

[1,3]Department of Electrical and Electronics Engineering, Jawaharlal Nehru Technological University, Hyderabad, India

Abstract: ***The proposed islanded hybrid renewable energy system integrates a photovoltaic array, a wind turbine, and a Battery at the Point of Common Coupling. Initially, the PV and wind inverters are controlled using a Fuzzy Logic Controller, which utilizes the DC-link voltage, DC power, and AC power as input variables to generate PWM gating signals for the inverters. These signals controls the inverter output voltage, frequency, and power delivered to the PCC. However, the performance of the conventional FLC depends heavily on predefined membership functions and expert-designed fuzzy rules, limiting its adaptability under varying operating conditions. To overcome these limitations, an Adaptive Neuro-Fuzzy Inference System is proposed. The ANFIS is trained with the backpropagation algorithm with FLC generated data, enabling automatic tuning of the controller parameters. Consequently, the proposed ANFIS based controller improves control accuracy, enhances active power transfer from the PV array, wind turbine, and BESS, and significantly reduces total harmonic distortion, resulting in superior power distribution and under varying operating conditions of the environment.***

Keywords: PV array, Wind, PMSG, BESS, MPPT, ANFIS, FLC, BP algorithm

Nomenclature

IMS	Islanded microgrid system
FLC	Fuzzy logic controller
MPPT	Maximum power point tracking
PV	Photo voltaic
ANFIS	Adaptive neuro fuzzy inference system
PCC	Point of common coupling
P & O	Perturb & Observe
BESS	Battery energy storage system
PMSG	Permanent magnet synchronous generator
VSI	Voltage source inverter

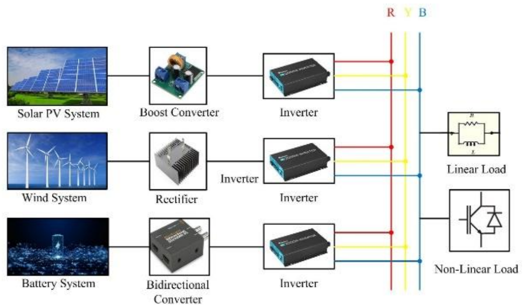

Figure 1: Schematic diagram of Islanded Microgrid system

1. Introduction

As renewable energy sources are being used more widely in electrical power systems, advanced control strategies are required to keep hybrid energy systems operating reliably and efficiently. In this context, islanded microgrids have emerged as a significant solution for modern power systems. By operating independently of the main utility grid, they can provide a continuous and reliable power supply to local loads using distributed energy resources [1,2]. Islanded microgrids provide an efficient platform for integrating hybrid energy resources such as PV array, wind turbines and battery. Clean energy contributes to lowering fossil fuel consumption while supporting sustainable power generation. Islanded microgrid systems (IMS) are particularly beneficial in remote and rural regions where extending the conventional utility grid is technically difficult and economically costly [3,4]. By generating electricity close to the point of consumption, they offer a reliable, practical, and cost-effective solution for supplying power to isolated communities [5,6].

The hybrid system integrates a PV array, wind turbine, and battery energy storage system (BESS) at the point of common coupling (PCC) as shown in Fig.1 [7,8]. The PV array is interfaced with the boost converter and a voltage source inverter (VSI) [9,10]. A perturb & observe (P & O) based maximum power point tracking (MPPT) algorithm is used to extract maximum solar power [11]. A fuzzy logic controller (FLC) utilizes the DC-link voltage (Vdc) and active power variation (ΔP) as input variables. Based on a predefined rule base, the controller generates the reference AC voltage (Vac) and frequency signals for inverter operation.

The wind turbine is mechanically coupled to a permanent magnet synchronous generator (PMSG) to produce variable-frequency AC power [12,13]. The rectifier converts AC output voltage into DC output voltage. A P&O based algorithm is employed to extract the maximum power from the wind turbine. The MPPT controller generates the switching signal for the boost converter, which regulates the DC-link voltage. The inverter is controlled by a FLC, which uses the DC-link voltage (Vdc), DC power (Pdc), and AC power (Pac) as input signals. Based on these inputs, the FLC produces PWM gating pulses for the inverter to deliver the required voltage and active power to the point of PCC.

The BESS is connected to a bidirectional boost converter, whose output is fed to the inverter [14,15]. A PID controller is employed to regulate the inverter operation by generating the required switching signals. The inverter supplies the required AC voltage and active power to the PCC. The BESS supports the microgrid by maintaining voltage stability, compensating for power variations, and sharing the load demand.

The hybrid microgrid produces variable power due to changing renewable energy availability, changing solar irradiance, wind conditions, and battery operating limits. An energy management system coordinates the PV array, wind turbine, and battery to maintain a balanced power supply [15,16]. Excess renewable energy is stored in the battery during high-generation periods, while stored energy is utilized during power shortages. The coordinated control of PV, wind, and battery systems enables efficient power sharing and stable microgrid operation. Intelligent control techniques maintain voltage and frequency within acceptable limits while minimizing power quality issues.

Conventional droop control is a traditional decentralized primary control technique widely employed in islanded microgrids to share power among distributed generation (DG) units [17]. However, it suffers from voltage and frequency deviations, inaccurate reactive power sharing due to line impedance mismatches, and slow dynamic response under load variations [18].To improve system stability and power quality, virtual impedance-based techniques such as virtual resistance and virtual conductance are employed [19, 20]. A Fuzzy Logic Controller (FLC) based control scheme is proposed to manage fluctuations in generation and load, providing greater adaptability and superior performance than conventional PI controllers [21,22].

The subsequent sections of this article are arranged in the following manner, **Section 2** presents the overall concept of an FLC based voltage, frequency control and power angle control in IMS, the **Section 3** presents proposed model of ANFIS implementation in IMS, architecture of back propagation algorithm, training of ANFIS and data sets, the **Section 4** demonstrates results and comparative analysis fuzzy and ANFIS control strategies, the **Section 5** summarizes the conclusion and future scope.

2. Existing Control strategies

The PV generation system employs an MPPT controlled boost converter to maximize solar energy extraction and maintain the DC-link voltage as shown in Fig.2. A voltage source inverter interfaced with a fuzzy logic controller regulates the PCC voltage and system frequency by dynamically adjusting the inverter control signals using voltage and frequency control method [23]. Consequently, the system achieves enhanced voltage stability, frequency regulation, and power quality under fluctuating solar irradiance and load conditions.

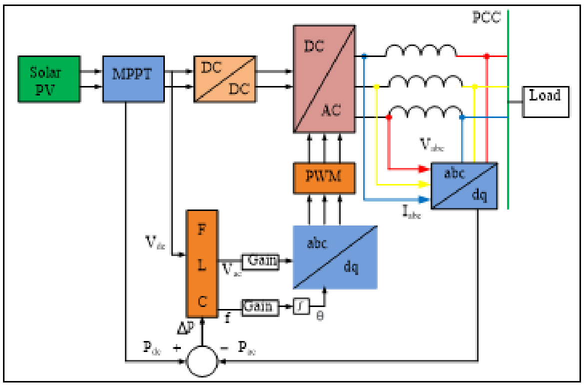

Figure 2: Schematic diagram of voltage and frequency control

The wind system consists of PMSG, Boost converter, and inverter as shown in Fig.3 [24,25]. The FLC is used to regulate the power angle during variations in renewable power generation. The reference power obtained from the MPPT algorithm is compared with the measured active power to calculate the power error. This error, along with the terminal voltage and system frequency, is provided as input to the controller [23]. Based on these inputs, the controller generates the reference AC voltage for the inverter, enabling power sharing under changing environmental conditions.

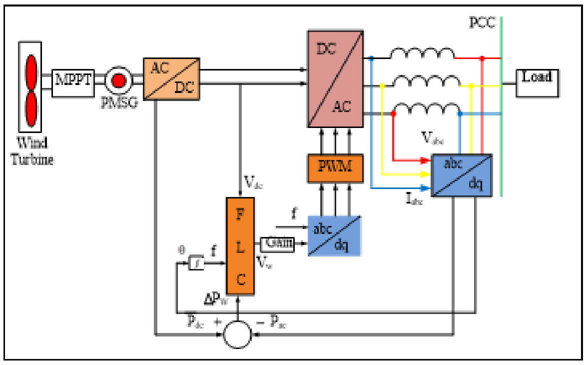

Figure 3: Schematic diagram power angle control scheme

Fuzzy logic controllers are widely used in renewable energy systems because they can effectively control nonlinear systems without requiring an accurate mathematical model. However, their performance mainly depends on the selection of membership functions and fuzzy rules, which may not provide the desired response under changing operating conditions. To overcome these limitations, an ANFIS is employed, automatically learns and updates the fuzzy rule base using training data, reducing the need for manual tuning. As a result, it improves controller adaptability, enhances dynamic performance of the system.

3. Development of ANFIS controller for IMS

An Adaptive Neuro-Fuzzy Inference System (ANFIS) controlled methodology is proposed to use inverters, which improves voltage regulation, frequency, and power control under different operating conditions. The ANFIS controller is trained using system data sets and subsequently employed for inverter switching and power regulation. Compared with the traditional FLC, the proposed ANFIS approach provides faster dynamic response, reduced steady-state error, improved DC-link voltage regulation, enhanced active and

Paper ID: SR26719231027 DOI: https://dx.doi.org/10.21275/SR26719231027

reactive power management, and better system stability under varying renewable energy and load conditions. Therefore, ANFIS offers a more intelligent and adaptive control solution for modern hybrid renewable energy systems.

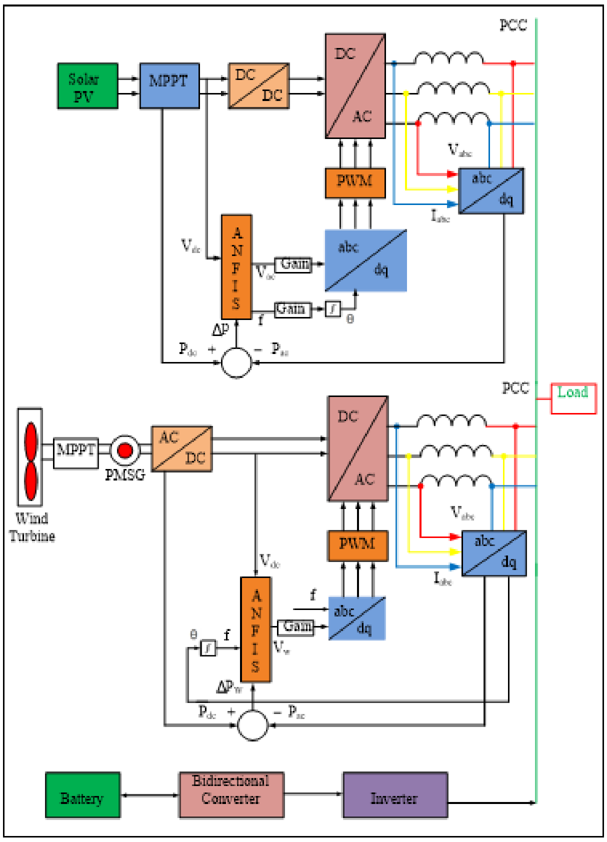

Figure 4: Overall block diagram of the system

3.1 Architecture of ANFIS

The Adaptive Neuro-Fuzzy Inference System (ANFIS) combines the human-like reasoning capability of fuzzy logic with the adaptive learning ability of artificial neural networks. In an islanded microgrid, ANFIS is employed to generate an appropriate control signal by continuously adapting its parameters according to system operating conditions. The controller consists of five computational layers, where each layer performs a specific function in the fuzzy inference process as shown in Fig.5.

In the proposed architecture, two input variables are applied to the ANFIS controller. Each input is represented by three membership functions, producing nine fuzzy rules. These rules are evaluated through the network, and the final output is obtained after aggregation and defuzzification.

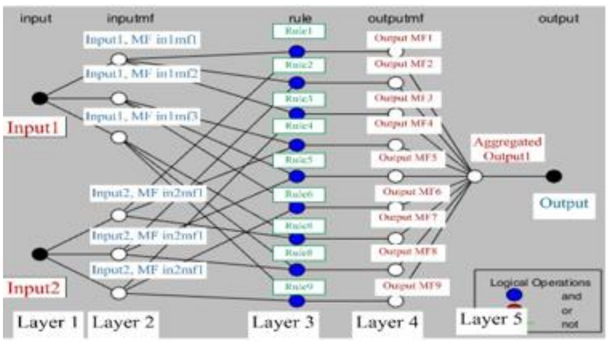

Figure 5: Architecture of ANFIS

Layer 1: Fuzzification Layer
The first layer converts the crisp input values into fuzzy values using predefined membership functions.
For two inputs x and y,

$$O_i^1 = \mu A_i(x), i = 1,2,3$$

$$O_i^1 = \mu B_{i\_3}(Y), i = 4,5,6$$

Where
- x, y are the controller inputs,
- A_i, B_i denote fuzzy sets,
- μ is the membership function.

A commonly used generalized triangular membership function is
- a = left endpoint
- b = peak point
- c = right endpoint

These parameters are called **premise parameters**.

The mathematical expression is

$$\mu(x) = \begin{cases} 0, & x \leq a \\ \frac{x-a}{b-a}, & a < x \leq b \\ \frac{c-x}{c-b}, & b < x < c \\ 0, & x \geq c \end{cases}$$

where
- $\mu(x)$is the membership grade,
- $x$is the input value.

The membership grade always lies between **0 and 1**

Layer 2: Rule Layer
Each node represents one fuzzy rule.

The firing strength of each rule is calculated by multiplying the corresponding membership grades.

$$w_i = \mu_{A_i}(x) \times \mu_{B_i}(y)$$

This layer performs the fuzzy AND operation.

Layer 3: Normalization Layer
Each rule firing strength is normalized as

$$\bar{w}_i = \frac{w_i}{\sum_{j=1}^{n} w_j}$$

Where
- n is the total number of fuzzy rules.

The normalized firing strengths satisfy

$$\sum_{i=1}^{n} \bar{w}_i = 1$$

Layer 4: Consequent Layer
Each node computes the rule output.
For a first-order Sugeno model,

$$f_i = p_i x + q_i y + r_i$$

Where
- $p_i, q_i, r_i$are consequent parameters.

The output becomes

$$O_i^{(4)} = \bar{w}_i f_i$$

Layer 5: Output Layer
The final ANFIS output is obtained by summing all rule outputs.

$$\text{Output} = \sum_{i=1}^{n} \bar{w}_i f_i$$

This output is supplied as the control signal to regulate the islanded microgrid.

Backpropagation Algorithm for ANFIS
Backpropagation is used to update the **premise parameters** of the membership functions so that the output error is minimized.

Step 1: Initialize Parameters
Initialize Membership function parameters a, b, c and consequent parameters p_i, q_i, r_i.

Step 2: Forward Pass
For each training sample, Calculate membership values, Compute firing strengths, Normalize firing strengths, Calculate rule outputs.
Obtain ANFIS output $\hat{y}$

Step 3: Compute Error
The error is

$$E = \frac{1}{2}(y - \hat{y})^2$$

Where
- y is the desired output,
- $\hat{y}$ is the ANFIS output.

Step 4: Backward Pass
The gradient of the error with respect to each premise parameter is calculated using the chain rule.

For any parameter θ,

$$\frac{\partial E}{\partial \theta} = \frac{\partial E}{\partial \hat{y}} \frac{\partial \hat{y}}{\partial w_i} \frac{\partial w_i}{\partial \mu} \frac{\partial \mu}{\partial \theta}$$

where $\theta \in \{a, b, c\}$

Step 5: Parameter Update
The parameters are updated using gradient descent.

$$\theta^{new} = \theta^{old} - \eta \frac{\partial E}{\partial \theta}$$

Where
- η is the learning rate.

Step 6: Repeat
Repeat the forward and backward passes until
- The error reaches the desired tolerance, or
- The maximum number of epochs is achieved.

3.2 Training of ANFIS:

Training of ANFIS membership functions for two input variables as shown in fig.6. The two input variables are delp and V_{dc}. For each input variable having the three membership functions and the rules for two input variables as shown in table.1 and 2.

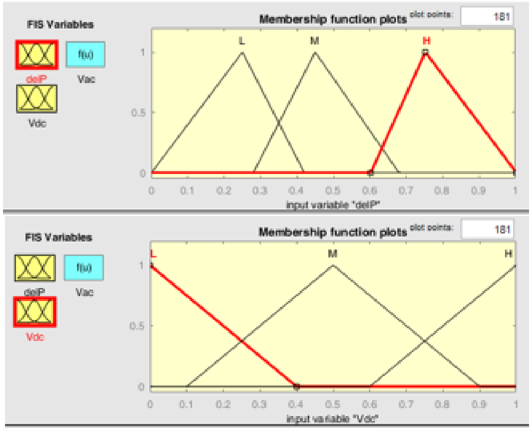

Figure 6: Membership functions for two input variables

Table 1: Rule set for Delp:

Rule1	If (delP is H) and (Vdc is H) then (Vac is H)
Rule2	If (delP is H) and (Vdc is M) then (Vac is M)
Rule3	If (delP is H) and (Vdc is L) then (Vac is M)
Rule4	If (delP is M) and (Vdc is H) then (Vac is M)
Rule5	If (delP is M) and (Vdc is M) then (Vac is M)
Rule6	If (delP is M) and (Vdc is L) then (Vac is L)
Rule7	If (delP is L) and (Vdc is H) then (Vac is L)
Rule8	If (delP is L) and (Vdc is M) then (Vac is L)
Rule9	If (delP is L) and (Vdc is L) then (Vac is L)

Table 2: Rule set for Vdc:

Rule1	If (delP is H) and (Vdc is H) then (Vac is H)
Rule2	If (delP is H) and (Vdc is M) then (Vac is M)
Rule3	If (delP is H) and (Vdc is L) then (Vac is M)
Rule4	If (delP is M) and (Vdc is H) then (Vac is M)
Rule5	If (delP is M) and (Vdc is M) then (Vac is M)
Rule6	If (delP is M) and (Vdc is L) then (Vac is L)
Rule7	If (delP is L) and (Vdc is H) then (Vac is L)
Rule8	If (delP is L) and (Vdc is M) then (Vac is L)
Rule9	If (delP is L) and (Vdc is L) then (Vac is L)

3.3 The proposed ANFIS Data sets:

Input 1: V_{dc}(DC-link Voltage), Input 2: ΔP(Change in Power) and three separate outputs are ANFIS-1 V_{ac}, ANFIS-2 f, ANFIS-3 P.Proposed system has three training datasets, each having the same inputs but a different target output. Below is a typical dataset values are shown in table.3,4 and 5. The values are physically consistent with a hybrid PV–wind–battery inverter operating around a 700 V DC bus.

Table 3: Dataset for ANFIS-1 (Output = AC Voltage)

Sample	(V_{dc}) (V)	(ΔP) (kW)	Target (Vac) (V)
1	650	-1.5	215
2	660	-1.2	218
3	670	-0.8	221
4	680	-0.5	224
5	690	-0.2	227
6	700	0.0	230
7	705	0.2	230
8	710	0.4	231
9	715	0.6	232
10	720	0.8	233
11	725	1.0	234
12	730	1.2	235
13	695	-0.4	228
14	705	-0.3	229
15	710	0.1	230

Paper ID: SR26719231027 DOI: https://dx.doi.org/10.21275/SR26719231027

Table 4: Dataset for ANFIS-2 (Output = Frequency):

Sample	(V_{dc}) (V)	(ΔP) (kW)	Target Frequency (Hz)
1	650	-1.5	49.30
2	660	-1.2	49.45
3	670	-0.8	49.60
4	680	-0.5	49.75
5	690	-0.2	49.90
6	700	0.0	50.00
7	705	0.2	50.01
8	710	0.4	50.03
9	715	0.6	50.05
10	720	0.8	50.08
11	725	1.0	50.10
12	730	1.2	50.12
13	695	-0.4	49.95
14	705	-0.3	49.98
15	710	0.1	50.00

Table 5: Dataset for ANFIS-3 (Output = Active Power)

Sample	(V_{dc}) (V)	(ΔP) (kW)	Target Power (kW)
1	650	-1.5	3.5
2	660	-1.2	3.8
3	670	-0.8	4.1
4	680	-0.5	4.3
5	690	-0.2	4.6
6	700	0.0	5.0
7	705	0.2	5.2
8	710	0.4	5.4
9	715	0.6	5.6
10	720	0.8	5.8
11	725	1.0	6.0
12	730	1.2	6.2
13	695	-0.4	4.8
14	705	-0.3	4.9
15	710	0.1	5.1

Table 6: Typical hybrid renewable energy System parameters

PV Aarry		Wind Turbine		Battery	
Power	2.4 Kw	Power	2.4 Kw	Rating	9 Kwh
Irs	1000 W/m^2	Density	1.25 Kg/m^3	L_b	0.1 e-3
Q	1.602×10^{-19} C	radius	1.31 m	C_p	12000 e^{-6}
θ	298 K	V_w	12 m/s	Lifecycle	> 10,000
Isrc	8.12 A	η_{gear}	1	Lifetime	5- 8 Years
N_s (series Strings)	12	P(Pole Pairs)	4	Q rated	30 Ah
N_p(Parallel Strings)	1	ω rated	2300 rpm	SOC	60%

Table.6 presents the parameters used for modelling the proposed hybrid renewable energy system. The simulation model is developed using these specifications, and all the results are obtained based on the parameter values listed in Table. 6. The selected parameters represent practical operating conditions and ensure reliable evaluation of the proposed ANFIS-based energy management and harmonic reduction strategy under islanded microgrid operation.

4. Simulation Results and Discussion

The typical proposed system is simulated for a duration of 1.3 s. Fig. 7(a), Fig. 7(b), and Fig. 7(c) present the maximum output voltage, maximum current, and maximum power extracted from the PV array using the perturb and observe (P&O) MPPT algorithm, respectively. Similarly, Fig. 7(d), Fig. 7(e), and Fig. 7(f) illustrate the maximum output voltage, maximum output current, and maximum power obtained from the wind energy conversion system using the same MPPT technique.

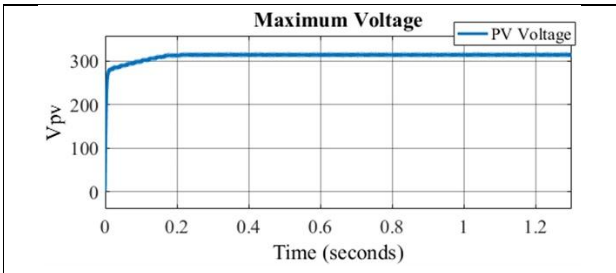

(a)

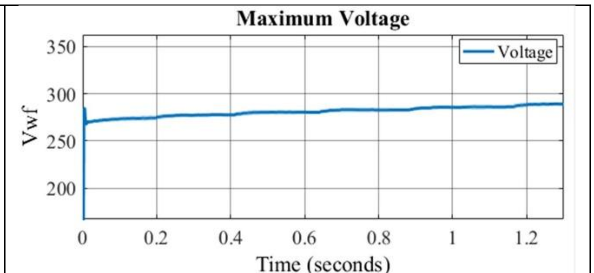

(d)

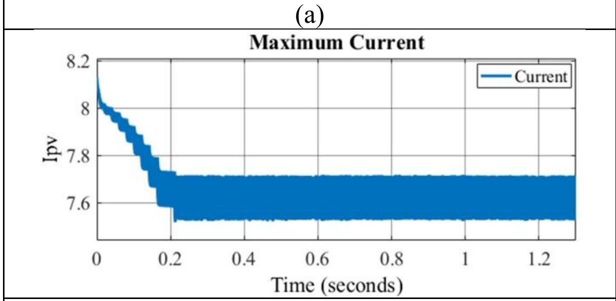

(b)

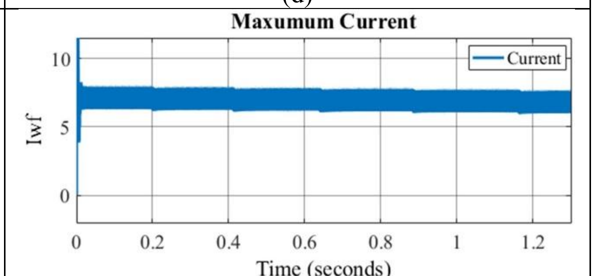

(e)

Paper ID: SR26719231027 DOI: https://dx.doi.org/10.21275/SR26719231027

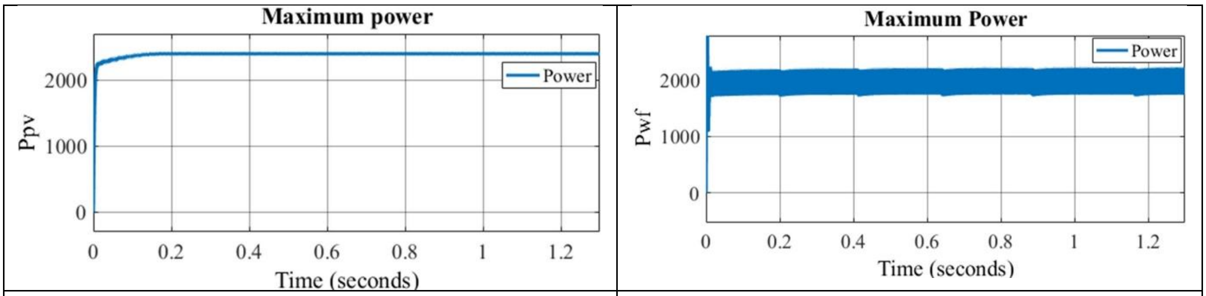

(c) (f)

Figure 7: (a) PV array maximum voltage, (b) PV array maximum current, (c) PV array maximum power, (d) Wind turbine maximum voltage, (e) Wind turbine maximum current, (f) Wind turbine maximum power

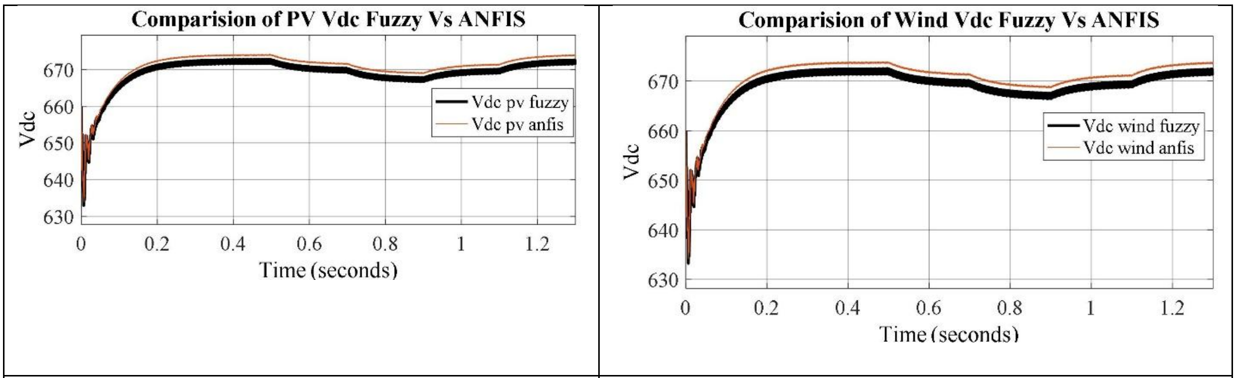

(a) (b)

Figure 8: (a) Comparison pv array DC voltage with Fuzzy and ANFIS , (b) Comparison wind turbine DC voltage with Fuzzy and ANFIS

A comparative analysis is carried out between the fuzzy logic controller and the Adaptive Neuro-Fuzzy Inference System. Comparison of PV array DC voltage with fuzzy and ANFIS as shown in in Fig. 8(a) and comparison of wind turbine DC voltage with fuzzy and ANFIS as shown in Fig. 8(b).

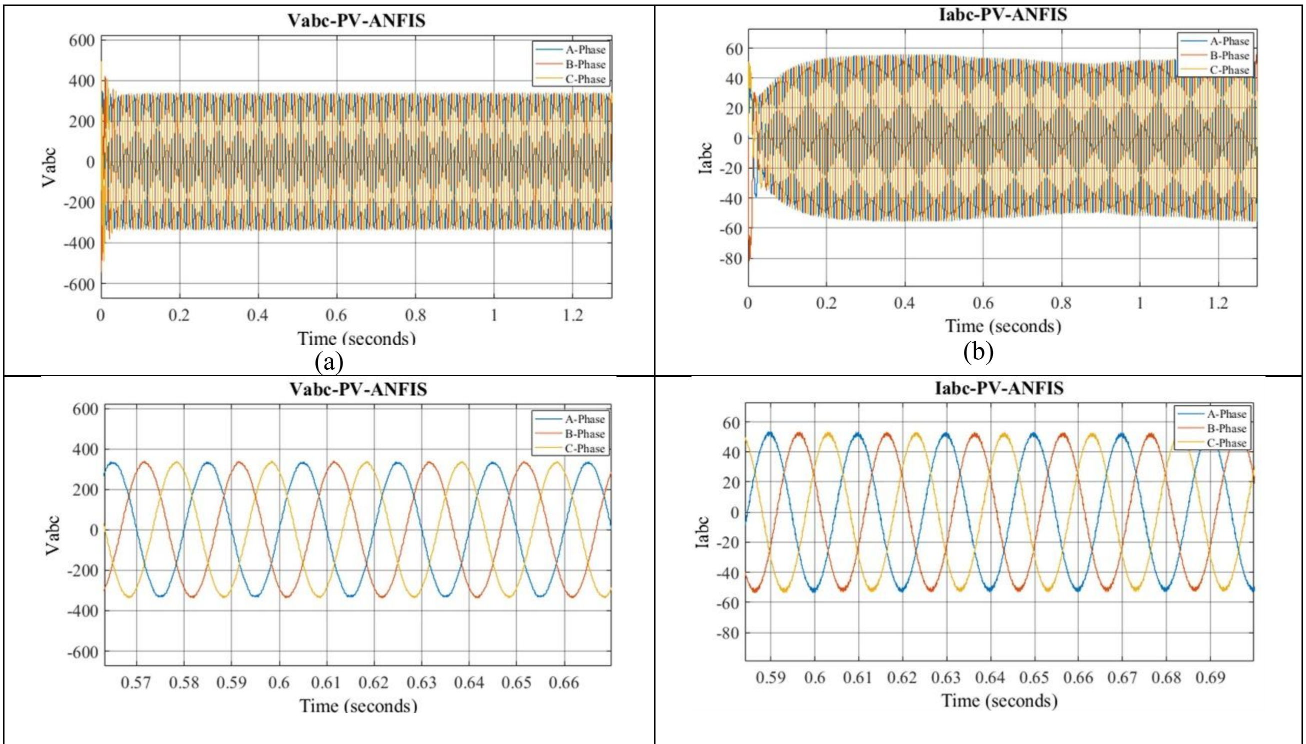

(c) (d)

Figure 9: (a)PV array output voltage of inverter, (b) PV array output current of inverter, (c) Zoomed version of PV array output voltage of inverter, (d) Zoomed version of PV array output current of inverter

The Fig.9 (a) and Fig.9 (b) shows the PV array inverter output voltage, current and Fig. 9(c) and Fig.9 (d) shows the enlarged view of inverter output voltage and current. Both waveforms exhibit a smooth sinusoidal behaviour, indicating improved power quality with reduced harmonic distortion.

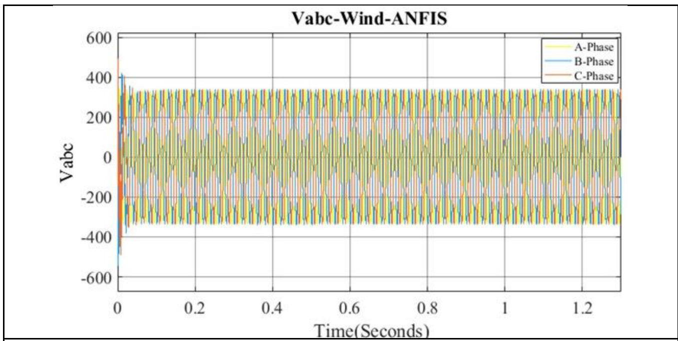

(a)

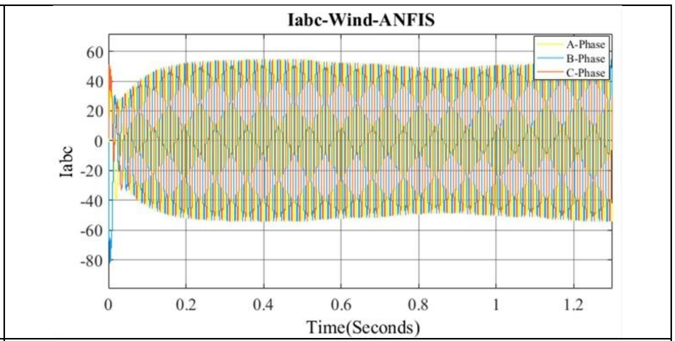

(b)

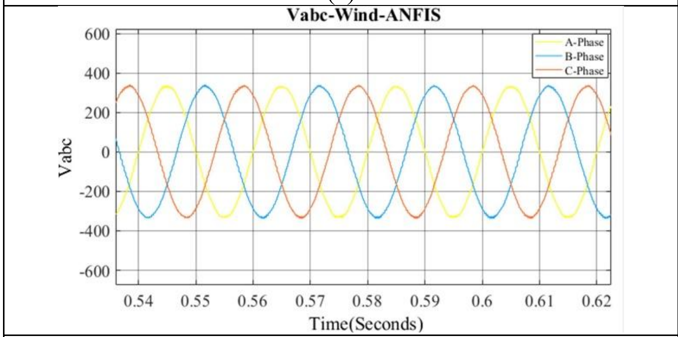

(c)

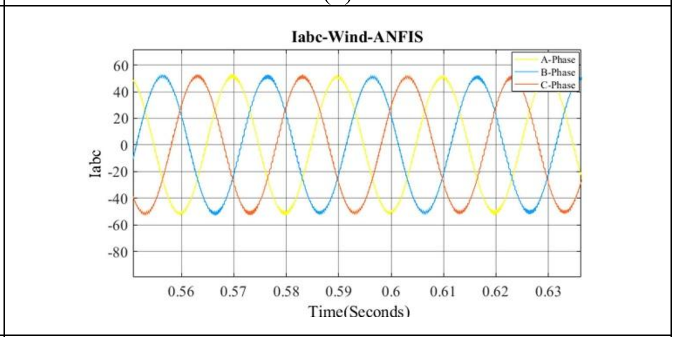

(d)

Figure 10: (a)Wind turbine output voltage of inverter, (b) Wind turbine output current of inverter, (c) Zoomed version of Wind turbine output voltage of inverter, (d) Zoomed version of Wind turbine output current of inverter

Wind turbine inverter output voltage, current as shown in Fig.10(a) and Fig.10(b).The zoomed version of wind turbine output voltage, current as shown in Fig.10(c) and Fig.10(d).The results demonstrates that sinusoidal and power quality is improved.

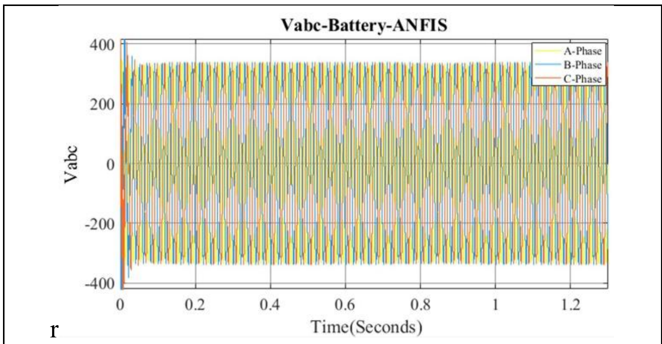

r

(a)

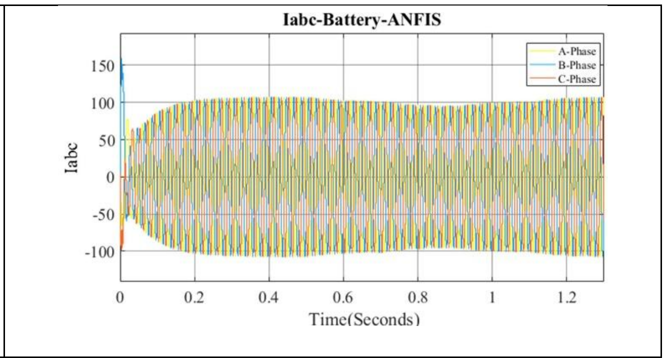

(b)

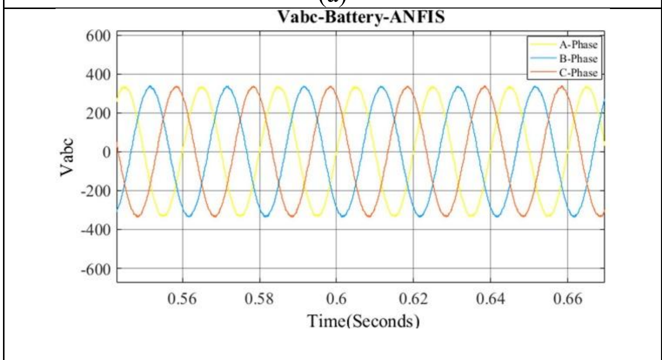

(c)

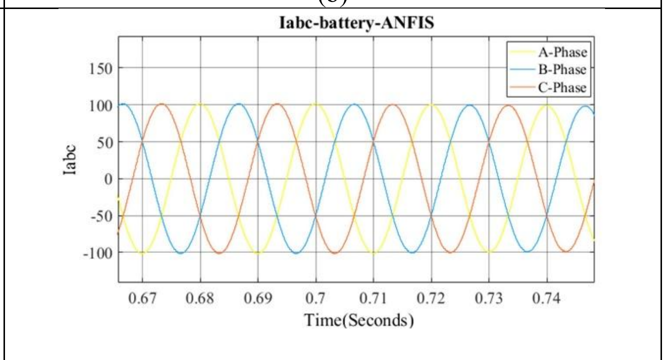

(d)

Figure 11: (a)Battery output voltage of inverter, (b) Battery output current of inverter, (c) Zoomed version of battery output voltage of inverter, (d) Zoomed version of battery output current of inverter

Paper ID: SR26719231027 DOI: https://dx.doi.org/10.21275/SR26719231027

The battery output voltage, current of inverter as shown in Fig.11(a) and Fig.11(b). The magnified version of voltage and current as shown in Fig.11(c) and Fig.11(d). The results demonstrate that the ANFIS controlled battery inverter maintains sinusoidal voltage and current.

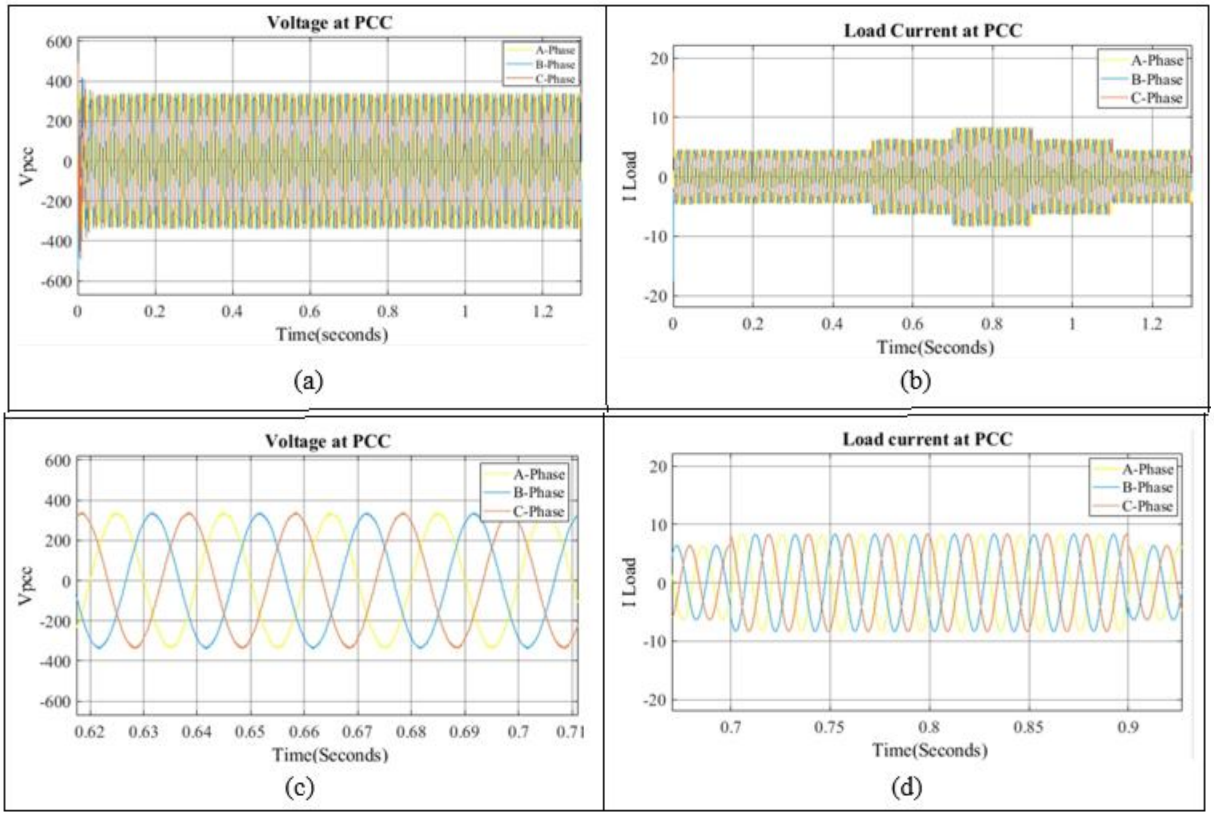

Figure 12 (a) Output voltage at PCC, (b) Load current at PCC, (c) Zoomed version of output voltage at PCC, (d) Zoomed version of load current at PCC

Output voltage at PCC, Load current as shown in Fig.12(a) and Fig.12(b). Fig. 12(c) and Fig. 12(d) provide enlarged views of the voltage and current waveforms for detailed observation.

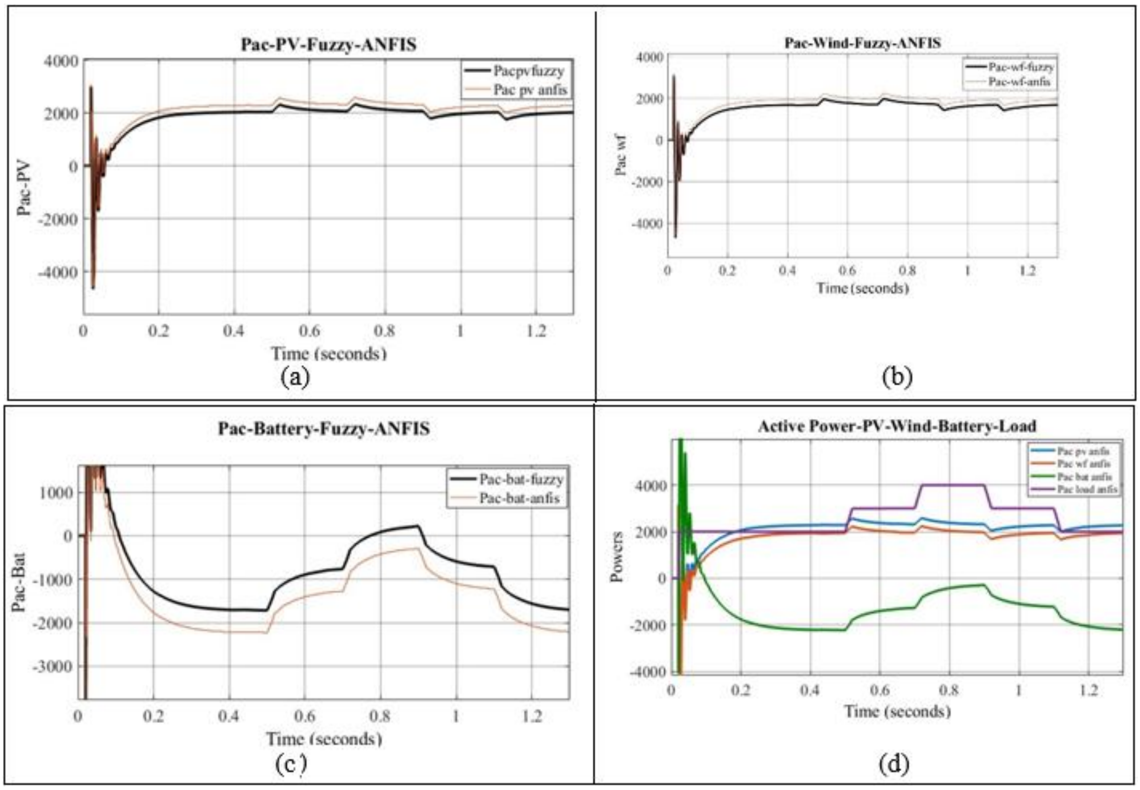

Figure 13: (a) comparison of pv array active power with Fuzzy and ANFIS,(b) comparison of wind turbine active power with Fuzzy and ANFIS, (c) comparison of battery active power with Fuzzy and ANFIS,(d) Active powers of pv array, wind turbine, battery and load

The active power generated by PV array, wind turbine using the ANFIS control strategy as shown in Fig.13(a) Fig.13(b).The battery charging and discharging power as shown in Fig.13(c) and Fig. 12(d) represents the active power delivered to the PCC under different operating conditions.

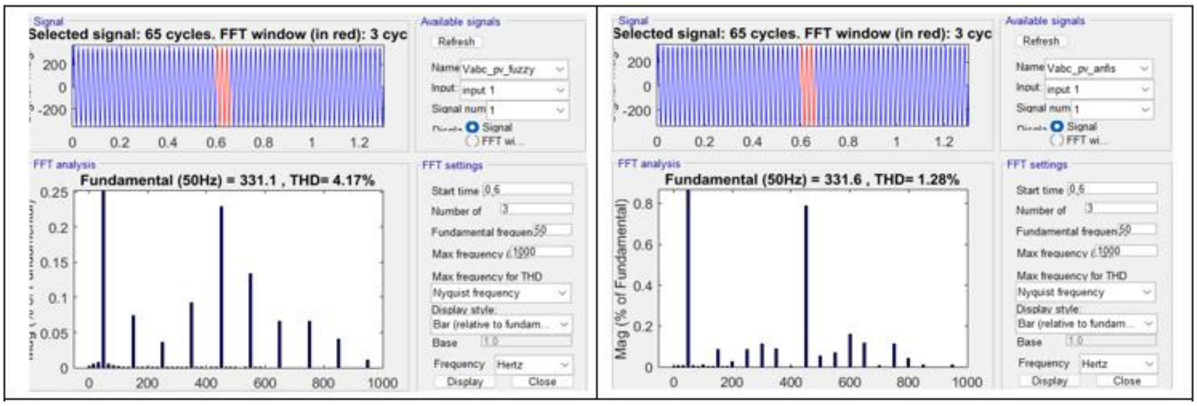

Figure 14: Comparison of total harmonic distortion in the PV array inverter output voltage under Fuzzy Logic and ANFIS-based control strategies.

In Fig.14 comparative analysis of output voltage of PV inverter with FLC and ANFIS. The simulation results show that the inverter output voltage controlled by the FLC has a THD of 4.1%, whereas the proposed ANFIS controller reduces the THD to 1.28%.

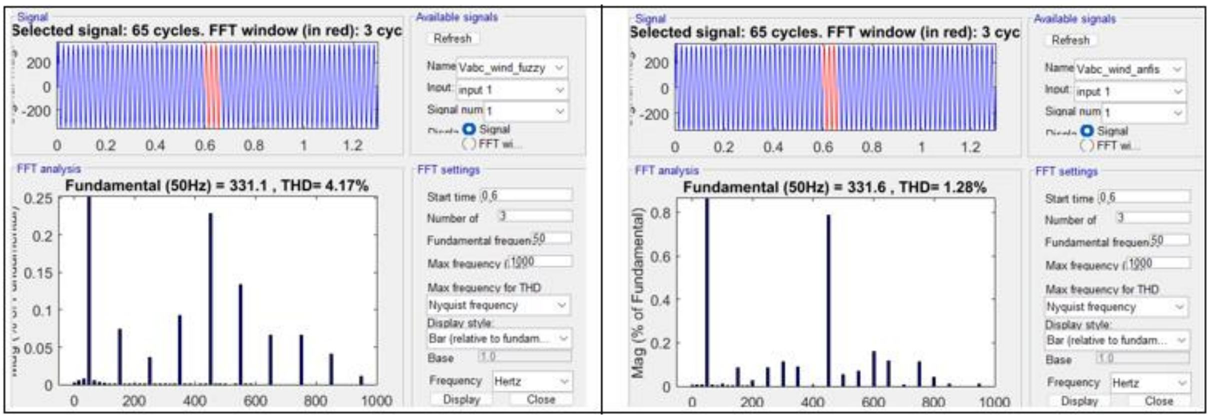

Figure 15: Comparison of total harmonic distortion in the Wind turbine inverter output voltage under Fuzzy Logic and ANFIS-based control strategies

In Fig.15 comparative analysis of output voltage of wind turbine with FLC and ANFIS. The simulation results show that the inverter output voltage controlled by the FLC has a THD of 4.17%, whereas the proposed ANFIS controller reduces the THD to 1.28%.

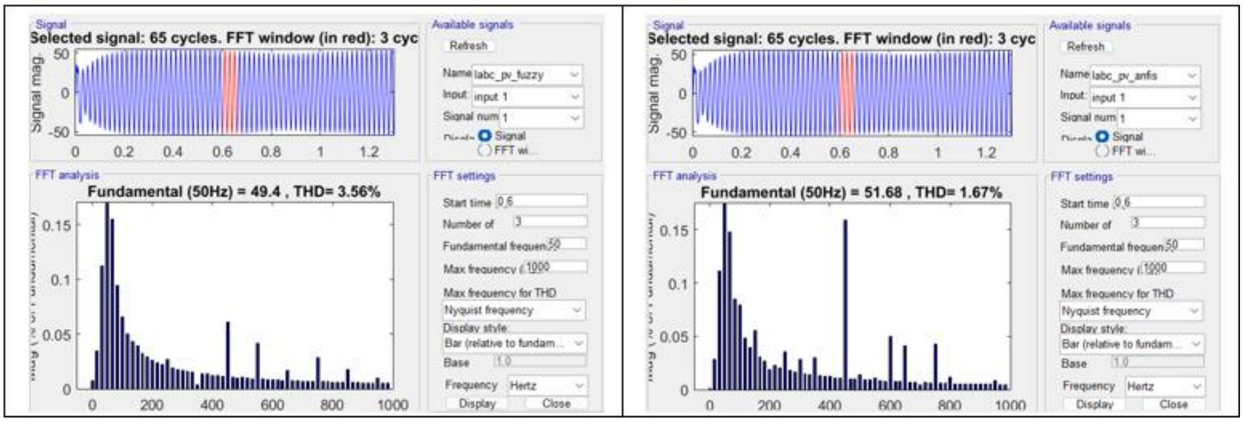

Figure 16: Comparison of total harmonic distortion in the PV array inverter output current under Fuzzy Logic and ANFIS-based control strategies.

In Fig.16 comparative analysis of output current of PV inverter with FLC and ANFIS. The simulation results show that the inverter output current controlled by the FLC has a THD of 3.56%, whereas the proposed ANFIS controller reduces the THD to 1.67%.

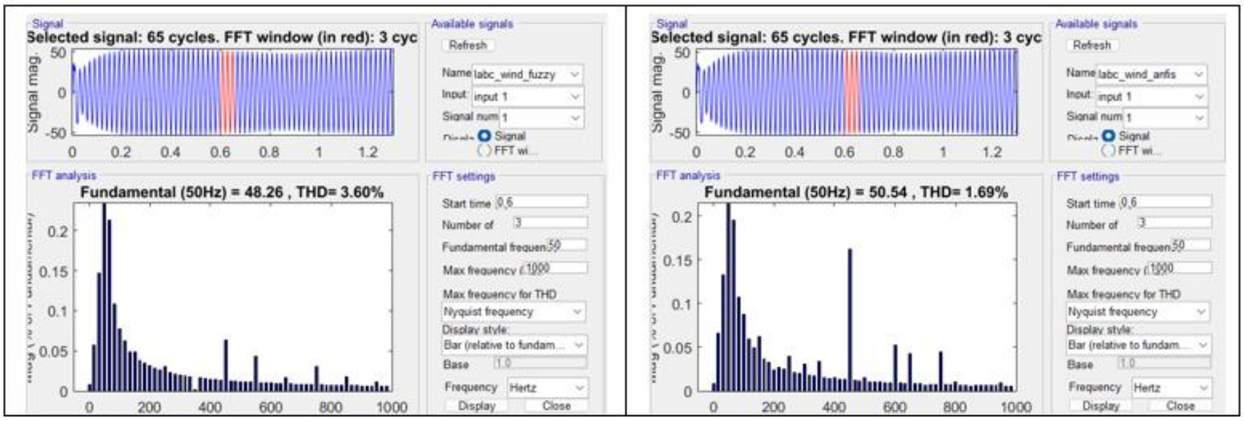

Figure 17: Comparison of total harmonic distortion in the Wind turbine inverter output current under Fuzzy Logic and ANFIS-based control strategies.

In Fig.16 comparative analysis of output current of wind turbine with FLC and ANFIS. The simulation results show that the inverter output current controlled by the FLC has a THD of 3.6%, whereas the proposed ANFIS controller reduces the THD to 1.69%.

5. Conclusion and Future scope

The ANFIS controller combines the learning capability of neural networks with the decision making process of fuzzy logic. This combination enables the controller to automatically adjust its response to variations in solar irradiance, wind speed, and load demand, resulting in improved adaptability under different operating conditions. The simulation results indicate that the proposed ANFIS-based control strategy provides more effective DC-link voltage regulation, improved active and reactive power management, quicker dynamic response, and lower power fluctuations than the conventional fuzzy logic controller. The battery energy storage system plays an important role in stabilizing the hybrid renewable energy system by compensating for renewable power variations, maintaining power balance, and supporting reliable system operation. The overall results demonstrate that the proposed ANFIS-based control approach is an efficient and adaptive solution for hybrid renewable energy systems, providing reliable operation and effective integration of renewable energy sources into modern power systems. The proposed ANFIS-based control strategy provides a practical solution for future microgrid and smart grid applications by improving power quality, ensuring stable system operation, and maximizing the utilization of renewable energy resources. Further work may involve testing the proposed ANFIS-based control strategy on real-time hardware and integrating advanced optimization techniques to improve control performance, energy management, and overall system efficiency.

References

[1] Shahgholian, Ghazanfar. "A brief review on microgrids: Operation, applications, modelling, and control." International Transactions on Electrical Energy Systems 31, no. 6 (2021): e12885.

[2] Punitha, S., N. P. Subramaniam, and P. Ajay D. Vimal Raj. "A comprehensive review of microgrid challenges in architectures, mitigation approaches, and future directions." Journal of Electrical Systems and Information Technology 11, no. 1 (2024): 60.

[3] Abbasi, Maysam, Ehsan Abbasi, Li Li, Ricardo P. Aguilera, Dylan Lu, and Fei Wang. "Review on the microgrid concept, structures, components, communication systems, and control methods." Energies 16, no. 1 (2023): 484.

[4] Fani, Bahador, Ghazanfar Shahgholian, Hassan Haes Alhelou, and Pierluigi Siano. "Inverter-based islanded microgrid: A review on technologies and control." E-prime-advances in electrical engineering, electronics and energy 2 (2022): 100068.

[5] Anderson, Alexander A., and Siddharth Suryanarayanan. "Review of energy management and planning of islanded microgrids." CSEE Journal of Power and Energy Systems 6, no. 2 (2019): 329-343.

[6] Ahmed, Ijaz, Muhammad Rehan, Abdul Basit, Hasnain Ahmad, Waqas Ahmed, Nasim Ullah, Marian Piecha, Vojtech Blazek, and Lukas Prokop. "Review on microgrids design and monitoring approaches for sustainable green energy networks." Scientific Reports 13, no. 1 (2023): 21663.

[7] Shivani, S., P. Rajendar, Dasari Sangeetha, Harshit Goud Naguluri, and Kalagotla Chenchireddy. "Efficiency Enhancement of Solar PV System Through MPPT and Boost Converter Design." In *2025 International Conference on Sustainable Communication Networks and Application (ICSCN)*, pp. 331-336. IEEE, 2025.

[8] Kumar, Raj, and S. K. Singh. "Solar photovoltaic modeling and simulation: As a renewable energy solution." *Energy Reports* 4 (2018): 701-712.

[9] Jenisha, C. Maria, N. Ammasai Gounden, and Anmol Agarwal. "Integration of PV array to three-phase grid using Power Electronic converters with de-coupled control." In 2018 20th National Power Systems Conference (NPSC), pp. 1-6. IEEE, 2018.

[10] Diouri, Omar, Najia Es-Sbai, Fatima Errahimi, Ahmed Gaga, and Chakib Alaoui. "Modeling and design of single-phase PV inverter with MPPT algorithm applied to the boost converter using back-stepping control in standalone mode." International Journal of Photoenergy 2019, no. 1 (2019): 7021578.

[11] Sneha, Tabitha, P. S. Kulkarni, Aaditya Rudra, and Soumya Deep Ghosh. "Design and Simulation of a Stand-Alone Hybrid Solar Photovoltaic-Fuel Cell-Battery System in MATLAB Simulink." In *2024 IEEE International Conference on Smart Power Control and Renewable Energy (ICSPCRE)*, pp. 1-6. IEEE, 2024.

[12] Zou, Ming, Yan Wang, Chengyong Zhao, Jianzhong Xu, Xiaojiang Guo, and Xu Sun. "Integrated equivalent model of permanent magnet synchronous generator-based wind turbine for large-scale offshore wind farm simulation." Journal of Modern Power Systems and Clean Energy 11, no. 5 (2023): 1415-1426.

[13] Beik, Omid, and Ahmad Al-Adsani. "Wind turbine productivity and wind energy assessment: An Ontario case study." In 2020 IEEE Electric Power and Energy Conference (EPEC), pp. 1-5. IEEE, 2020.

[14] Moncecchi, Matteo, Claudio Brivio, Stefano Mandelli, and Marco Merlo. "Battery energy storage systems in microgrids: Modeling and design criteria." Energies 13, no. 8 (2020): 2006.

[15] Szilagyi, E., D. Petreus, and T. Patarau. "Optimal energy management for an islanded microgrid with battery degradation cost considerations." In 2024 IEEE 30th International Symposium for Design and Technology in Electronic Packaging (SIITME), pp. 1-6. IEEE, 2024.

[16] Sreelekshmi, R. S., Rishika Lakshmi, and Manjula G. Nair. "AC microgrid with battery energy storage management under grid connected and islanded modes of operation." Energy Reports 8 (2022): 350-357.

[17] Pham, Xuan Hoa Thi. "Power sharing strategy in islanded microgrids using improved droop control." Electric Power Systems Research 180 (2020): 106164.

[18] Sun, Qian, Qiuye Sun, and Dehao Qin. "Adaptive fuzzy droop control for optimized power sharing in an islanded microgrid." Energies 12, no. 1 (2018): 45.

[19] Kim, Sunghyok, Songchol Hyon, and Yongil An. "Harmonic power sharing control using adaptive virtual harmonic impedance in islanded Microgrids." International Journal of Emerging Electric Power Systems 25, no. 2 (2024): 135-148, degruyterbrill.com.

[20] Goh, Hui Hwang, Xiaofeng Zhang, Dongdong Zhang, Wei Dai, Jiefeng Liu, Gaoxiang Li, Tonni Agustiono Kurniawan, and Kai Chen Goh. "Harmonic virtual impedance control in islanded Microgrids for harmonic power sharing and harmonic suppression." CSEE Journal of Power and Energy Systems (2024), ieeexplore.ieee.org.

[21] Budahab, Wajdi, Mahmoud Hamouda, and Kamal Al-Haddad. "A fuzzy logic based controller of DC-link voltage regulation of parallel inverters operation during unintended islanding mode." In IECON 2017-43rd Annual Conference of the IEEE Industrial Electronics Society, pp. 7891-7896. IEEE, 2017.

[22] Kumari, Sushmita, H. M. Suryawanshi, D. Govind, P. P. Nachankar, and Chintalpudi L. Narayana. "A fuzzy logic based load shedding approach for islanding mode of microgrid." In 2021 IEEE international power and renewable energy conference (IPRECON), pp. 1-6. IEEE, 2021.

[23] Bhattacharya, Anagha, Debashis Chatterjee, and Swapan Kumar Goswami. "A fuzzy based improved power sharing methodology for islanded microgrid with hybrid sources." Electric Power Systems Research 217 (2023): 109069.

[24] Pinthurat, Watcharakorn, and Branislav Hredzak. "Fully decentralized control strategy for heterogeneous energy storage systems distributed in islanded DC datacentre microgrid." *Energy* 231 (2021): 120914.

[25] Rana, Nischay, and Alka Singh. "Control and Modelling of PMSG-Based Wind Turbine for Integration to Conventional Grid." In *2025 IEEE North-East India International Energy Conversion Conference and Exhibition (NE-IECCE)*, pp. 1-6. IEEE, 2025.

[26] Kulkarni, Haripriya, Amruta Kulkarni, Tejas Pagire, and Sadique Magdum. "Mathematical Modeling, Installation of Wind turbine and its analysis in MATLAB." In *2022 International conference on Electronics and renewable Systems (ICEARS)*, pp. 142-149. IEEE, 2022.